Structural and electronic properties of 3*d* transition metal impurities in silicon carbide

L. V. C. Assali,[1] W. V. M. Machado,[1] and J. F. Justo[2]
[1]*Instituto de Física, Universidade de São Paulo, Caixa Postal 66318, 05315-970 São Paulo, São Paulo, Brazil*
[2]*Escola Politécnica, Universidade de São Paulo, Caixa Postal 61548, CEP 05424-970 São Paulo, São Paulo, Brazil*
(Received 30 September 2003; revised manuscript received 11 December 2003; published 29 April 2004)

We carried out a theoretical investigation on the electronic and structural properties of typical residual transition metal impurities in silicon carbide. The calculations were performed using the all electron spin-polarized full-potential linearized augmented plane-wave methodology. The results on stability, spin states, hyperfine parameters, formation and transition energies of isolated Ti, V, and Cr impurities in 3*C*-SiC and 2*H*-SiC were compared to available experimental data.

DOI: 10.1103/PhysRevB.69.155212 PACS number(s): 61.72.Ww, 71.55.−i

I. INTRODUCTION

Silicon carbide (SiC) has been potentially considered in device technology for applications at high temperatures, high frequencies, and high powers.[1] SiC is a wide band-gap semiconductor which has more than 200 known polytypes.[2] From all these polytypes, interest has been focused on the cubic (3*C*) and hexagonal (4*H* and 6*H*) phases. Crystalline silicon carbide is generally grown by the Lely technique, in which residual impurities end up being incorporated in the material. Transition metals, such as titanium, vanadium, and chromium, are some of those impurities which have been identified in the resulting silicon carbide.[3] Since transition metals are known to generate electrically active centers in semiconductors, it is important to identify the properties of those impurities in SiC.

Vanadium and chromium generate active centers in all SiC polytypes. On the other hand, the activity of titanium depends on the host polytype. Experiments indicate that while Ti is active in 4*H*-SiC, it is inactive in 3*C*-SiC.[3] Although the local structure is essentially the same in either hexagonal or cubic material, the electronic activity of titanium should result from the differences in the materials band gap ε_g. Deep level transient spectroscopy experiments on Ti in 4*H*-SiC show that Ti introduces gap levels near the conduction-band bottom.[4] According to the Langer-Heinrich rule,[5] the transition energies of a transition metal (TM) are aligned with respect to a bulk reference level. The valence-band tops for both polytypes are essentially aligned, and ε_g is considerably smaller in 3*C*-SiC (2.42 eV) than in 4*H*-SiC (3.27 eV). Therefore, the Ti-related acceptor transition energy would be pinned in the conduction band for the 3*C*-SiC, and it would be undetectable.

To the best of our knowledge, so far there is no *ab initio* investigation on transition metals in silicon carbide in which atomic relaxations are taken into account. Here we carried out an investigation on the electronic and structural properties of Ti, V, and Cr in cubic (3*C*) and hexagonal (2*H*) silicon carbide. Hexagonal 2*H* silicon carbide is the prototypical crystalline configuration for device applications since it has the largest energy band gap from all polytypes (3.33 eV). Although growing 2*H* silicon carbide samples are still a remarkable task, for our theoretical investigations it is the ideal hexagonal polytype configuration since the crystal contains only one nonequivalent sublattice for either silicon or carbon atoms.

We carried our calculations using the spin-polarized full-potential linearized augmented plane-wave method.[6,7] We showed that TM impurities are energetically favorable in the silicon substitutional sublattice rather than in the carbon substitutional sublattice or interstitial sites in SiC. We computed the symmetry, spin, hyperfine parameters, and energetics of those centers in several charge states in 3*C*-SiC and 2*H*-SiC.

II. METHODOLOGY

The full-potential linearized augmented plane wave (Ref. 7) is one of the most accurate *ab initio* methods, and still computationally efficient, to investigate the electronic and structural properties of solids and its defects.[8] Within such methodology, the exchange-correlation potential was described by the density-functional theory[9,10] in the generalized gradient approximation.[11] Additionally, we used the spin-polarized and the relativistic scheme.

We considered a reference supercell of 54 atoms for the 3*C*-SiC crystal, in a face centered cubic Bravais lattice. The distance between an impurity and its images is 9.29 Å. Since our calculations involve only deep centers, this distance is enough to avoid relevant image interactions. We should stress that we also performed calculations with 32-atom supercells, which showed to be inappropriate for our investigation, mostly in the case of impurities sitting in interstitial sites. For the 2*H*-SiC crystal, we considered a reference supercell of 56 atoms, in a hexagonal Bravais lattice. The distance between an impurity and its images is 8.19 Å in basal plane direction and 10.11 Å in the normal direction.

For the bulk materials, a convergence in total energy was achieved using 5.8/R (maximum length of the plane waves), where R is the smallest radius of spheres which define the host atoms. We used $R_{Si}=1.5$ a.u. and $R_C=1.2$ a.u. In all calculations involving the TM impurities, we used $R_{TM}=1.2$ a.u. Self-consistent interactions were performed until convergence on both the total energy (10^{-4} eV per unit cell) and total charge in the atomic spheres (10^{-5} electronic charges per atom) were achieved. The atomic positions were relaxed using the damped Newton scheme until the forces were smaller than 1 mRy/a.u. The Brillouin zone (BZ) was sampled by a $2\times2\times2$ grid[12] and a unique k point in the

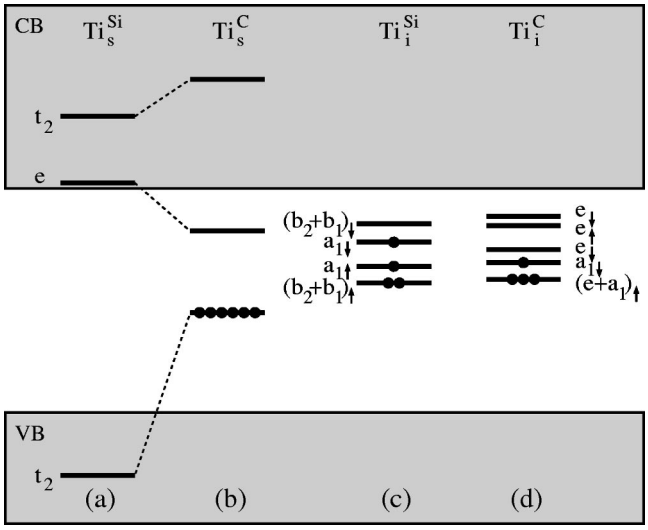

FIG. 1. Schematic representation of the Ti $3d$-related impurity energy levels, in the band-gap region for the neutral Ti_s^{Si}, Ti_s^{C}, Ti_i^{C}, and Ti_i^{Si} centers around the Γ point. The occupation of the energy-gap levels are represented by the numbers of full circles. The $\uparrow$ and $\downarrow$ arrows represent the spin-up and spin-down levels, respectively.

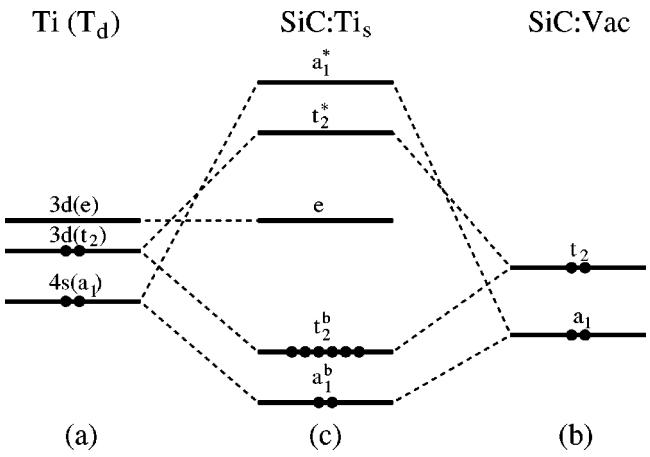

FIG. 2. Schematic representation of the crystal-field theory for the substitutional titanium impurity in a tetrahedral symmetry. The b and * symbols indicate the bonding and antibonding states, respectively. (a) $3d+4s$ titanium atomic states in T_d crystal field, (b) vacancy-related states in SiC, and (c) titanium-related states in substitutional site in $3C$-SiC.

center of the zone. For all the systems, we used the respective theoretical lattice parameters, as initially computed by the same methodology and equivalent sets of k points to sample the BZ. Those approximations lead to $a=4.38$ Å [$a_{expt}=4.360$ Å (Ref. 13)] in $3C$-SiC and $a=3.09$ Å and $c=5.05$ Å [$a_{expt}=3.076$ Å, $c_{expt}=5.035$ Å (Ref. 13)] in $2H$-SiC.

III. RESULTS

A. Titanium impurity in $3C$-SiC

Figure 1 displays the impurity-induced energy levels, based on the Kohn-Sham eigenvalues, for the neutral isolated Ti impurity in $3C$-SiC. Figures 1(a) and 1(b) show, respectively, the results for the impurity in substitutional Si (Ti_s^{Si}) and C (Ti_s^{C}) sites, and Figs. 1(c) and 1(d) the results for the tetrahedral interstitial Ti impurity surrounded, respectively, by four nearest-neighboring Si atoms (Ti_i^{Si}) and by four C atoms (Ti_i^{C}).

In $3C$-SiC, the Ti_s^{Si} center [Fig. 1(a)] introduces no energy levels in the band gap, showing an effective spin $S=0$ and a T_d point symmetry. The four nearest neighbors undergo an outward relaxation of only 0.1 Å. The Ti-related energy levels are unoccupied resonant levels in the conduction band. The crystal-field splitting between the e and the t_2 levels is 0.7 eV. The Ti_s^{C} center is also a closed-shell system [Fig. 1(b)], being stable in T_d point symmetry, where the four nearest-neighbor Si atoms and the 12 next-nearest-neighbor C atoms relax outward by 0.5 Å and 0.1 Å, respectively. However, this center displays a fully occupied t_2 level in the band gap. In contrast to the Ti_s^{Si} center, the interactions between Ti and the Si nearest-neighboring atoms cause a crystal-field splitting of 1.6 eV and the vacancy t_2-related energy level lies in the band gap. Our results for substitutional Ti are consistent with a recent theoretical investigation[14] if atomic relaxations are not taken into account. We should stress that relaxation plays a major role on the final results for Ti_s^{C}, even determining the spin ground state ($S=0$) of the center.

The crystal-field theory could be invoked to explain the results on the substitutional titanium impurity in a tetrahedral symmetry (Fig. 2). Although the Ti atom is isoelectronic with Si and C atoms, its electronegativity is 1.5 (in the Pauling scale), close to the value 1.8 for Si, but considerably lower than the value of 2.5 for C. Therefore, a different behavior of Ti atom could be expected if rebonding to nearest-neighboring Si or C atoms. Figure 2(b) presents a schematic representation of the electronic structure of a vacancy in SiC. A Si vacancy presents an acceptor character so the t_2 energy level, occupied by two electrons, is near the top of the valence band. On the other hand, a C vacancy presents a donor character and the t_2 energy level, occupied by two electrons, is near the bottom of the conduction band. Therefore, when a Ti atom replaces a Si atom, it undergoes a p-d hybridization, binding to the four carbon atoms. The reconstruction of the dangling bonds coming from the Si vacancy pushes the t_2-related vacancy levels down to the valence band, introducing a nonbonding orbital with an e symmetry and a t_2 antibonding level in the conduction band, as represented in Fig. 2(c). The introduction of the Ti impurity in the C vacancy reconstructs only slightly the dangling bonds, leaving a fully occupied t_2 vacancy-related energy level in the band gap. This model is clearly evidenced by the contour plot of the total electronic charge density shown in Fig. 3 for (a) Ti_s^{Si} center and (b) Ti_s^{C} center, in the neutral charge state. The figure shows that only the Ti_s^{Si} center presents large concentration of interstitial charge between Ti and its neighbors, an evidence of bond reconstruction. While there is a rebonding of the vacancy dangling bonds for substitutional Ti in a Si site [Fig. 3(a)], this is not observed for a substitutional Ti in a C site [Fig. 3(b)].

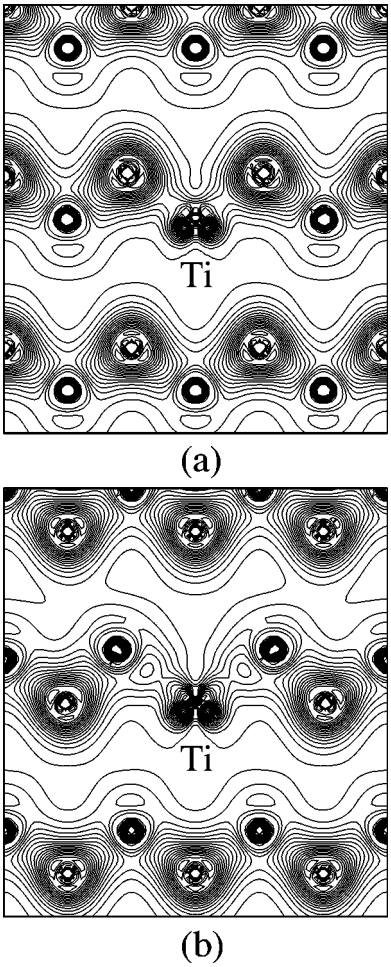

FIG. 3. Contour plot of the total electronic charge density in the [110] plane for (a) Ti_s^{Si} and (b) Ti_s^C in the neutral charge state. The line separation is 0.1 e/Å^3.

The Ti_i^{Si} center (interstitial Ti impurity surrounded by four nearest-neighboring Si atoms) presents a low-spin configuration, with an effective spin $S=1$ and a C_{2v} point symmetry, with the energy levels presented in Fig. 1(c). The four nearest-neighboring Si atoms relax outward by about 12%. Relevant relaxation was also observed on the fourth nearest-neighboring C atoms (by about 5%), which are those atoms bounded to the impurity first neighbors.

The Ti_i^C center presents a low-spin configuration with an effective spin $S=1$ in a C_{3v} point symmetry [Fig. 1(d)]. Relaxation takes place with the Ti impurity moving toward one of the C first neighbors by 0.11 Å, pulling this C atom to relax away in the same direction by 0.07 Å. The other three first neighbors also relax away from the Ti impurity by 0.12 Å. In this case, the distortion, lowering the symmetry of the center from T_d to C_{3v}, is important to determine the effective spin of the center. In the T_d symmetry, the center presents a high-spin configuration ($S=2$), but in the C_{3v} the spin is $S=1$. This result contrasts with the Ti_i^{Si} center, which presents a low-spin configuration in either symmetry.

Table I summarizes the results for the Ti impurities in $3C$-SiC. The table presents the symmetry, total spin, formation energies,[15,16] transition energies, and contact hyperfine parameters in the Ti nucleus for substitutional and interstitial centers in $3C$-SiC. Using the total energies for the centers in positive and negative charge states, we computed the respective donor and acceptor transition energies and formation energies (as explained in the Appendix). Since the Ti-related energy levels of Ti_s^{Si} center lie outside the band gap, the acceptor transition of this center does not exist, which is consistent with experimental measurements.[3,17] We find that the charge state of a certain center does not alter substantially the contact hyperfine terms. Additionally, the contact term is negligible for substitutional titanium.

The Ti_s^{Si} center has the lowest formation energy, being the preferential configuration in SiC. Formation energies for other Ti centers are at least 6.1 eV higher than the one of this configuration. It is energetically favorable for titanium to stay in sites with carbon atoms as first neighbors in all charged states. Therefore, in the following sections we focus our investigation only on the properties of Ti, V, and Cr sitting in the Si sublattice (TM_{Si}) in both $3C$-SiC and $2H$-SiC materials.

B. Transition metals in $3C$-SiC and $2H$-SiC

Figure 4 displays the energy eigenvalues representing the $3d$-related impurity levels in the band-gap region for the neutral substitutional Ti, V, and Cr in $3C$-SiC and $2H$-SiC. In $3C$-SiC, the $3d$-related energy levels are split into an e plus a t_2 representation, while in $2H$-SiC, due to the C_3 symmetry, the t_2 representation splits further into an e plus an a level. In the figure, the top of the valence bands in $3C$ and $2H$ polytypes were aligned, without any valence-band offset. This was justified by theoretical investigations which computed a small valence-band offset between $2H$- and $3C$-SiC (0.13 eV),[18] and also by experimental data in which a small valence-band offset was found between $4H$- and $6H$-SiC (0.17 eV).[19]

By comparing the Ti-related levels in $3C$ [Fig. 4(a)] and $2H$-SiC [Fig. 4(d)], we find that the nonbonding energy level with an e representation lies essentially at the same position with relation to ε_v. This unoccupied level lies inside the band gap in the $2H$ polytype, and has a higher d character when compared to the respective level in the $3C$ polytype. This center in $2H$-SiC has a C_3 point symmetry, with the four nearest neighbors undergoing an outward relaxation of about 6%.

The figure also presents the $3d$-related energy levels for neutral substitutional V and Cr in $3C$ and $2H$ polytypes. In both polytypes the V impurity introduces a partially occupied $e_\uparrow$ level in the center of the gap [Figs. 4(b) and 4(e)]. The Cr impurity introduces a fully occupied $e_\uparrow$ level in the lower half of the gap [Figs. 4(c) and 4(f)]. The energy-level ordering shows that the V center presents a low-spin configuration ($S=1/2$) while the Cr center presents a high spin configuration ($S=1$). As a result of the electronic configuration for V, an ^2E ground state can be assigned to the center, which should lead to a symmetry lowering. However, our calculations showed that distortions are very small, and the center remains essentially in a T_d symmetry. In terms of the structural relaxation, we find that for the V and Cr centers, the

TABLE I. Results for substitutional and interstitial titanium in 3*C*-SiC. The table presents the symmetry, total spin S, formation energies ΔE_f, transition energies E_t with relation to the valence-band top ε_v, and isotropic contact hyperfine term A in the ^{49}Ti nucleus. Energies and hyperfine parameters are given in eV and MHz, respectively. The theoretical approximations and numerical truncations lead to an estimated error of ≈ 0.2 eV in the calculated transition energies and ≈ 1 MHz in the hyperfine terms. ε_F is the Fermi energy and $0 \leqslant \gamma \leqslant 1$, where $\gamma=0$ and $\gamma=1$ describe the silicon and carbon rich environments, respectively. All the formation energies are presented with relation to the $(Ti_s^{Si})^0$ center, which is 4.3 eV.

	Symmetry	S	ΔE_f	E_t	A
$(Ti_s^{Si})^0$	T_d	0	0.0		0
$(Ti_s^{C})^+$	C_{2v}	1/2	$6.1+1.2\gamma+\varepsilon_F$	1.1(0/+)	−1
$(Ti_s^{C})^0$	T_d	0	$7.2+1.2\gamma$		0
$(Ti_s^{C})^-$	D_{2d}	1/2	$9.2+1.2\gamma-\varepsilon_F$	2.0(0/−)	1
$(Ti_i^{Si})^+$	T_d	3/2	$6.1+0.6\gamma+\varepsilon_F$	2.0(0/+)	−16
$(Ti_i^{Si})^0$	C_{2v}	1	$8.1+0.6\gamma$		−15
$(Ti_i^{Si})^-$	C_{2v}	1/2	$10.2+0.6\gamma-\varepsilon_F$	2.1(0/−)	−16
$(Ti_i^{C})^+$	C_{3v}	3/2	$4.3+0.6\gamma+\varepsilon_F$	1.8(0/+)	−8
$(Ti_i^{C})^0$	C_{3v}	1	$6.1+0.6\gamma$		−9
$(Ti_i^{C})^-$	C_{3v}	1/2	$8.0+0.6\gamma-\varepsilon_F$	1.9(0/−)	−9

four nearest neighbors undergo outward relaxation of about 3% in both 3*C* and 2*H* polytypes.

Table II summarizes the symmetry, total spin, formation energies, transition energies, and contact hyperfine parameters for TM_{Si} in 3*C*-SiC and 2*H*-SiC in several charge states. From the Ti^0 to the Cr^0 impurities in 3*C*-SiC, the crystal symmetry is kept $[T_d]$, while for Cr^- there is a symmetry lowering to C_{3v}. To understand such a behavior, Fig. 5 presents the energy eigenvalues for the Cr center in several charge states. For the Cr^+ and Cr^0 centers in both polytypes, the last occupied level has a nonbonding 3*d*-character (*e* state) with a high 3*d* electronic concentration inside the Cr sphere. However, the energy-level ordering is such that the Cr^+ centers present a low-spin configuration, while the Cr^0 centers present a high-spin configuration. The last occupied level in the Cr^- center in 3*C*-SiC [Fig. 5(c)] has an antibonding character and is represented by an energy level with a_1 representation. That a_1 level came from the splitting of the t_2 level when the symmetry of the center was lowered from T_d to C_{3v}, resulting in a high-spin configuration. The same is observed for Cr^- center in 2*H*-SiC, but the levels with an antibonding character have a high 3*d* electronic concentration inside the Cr sphere. For the Cr^{2-} in 3*C*-SiC [Fig. 5(d)], the center is in a T_d symmetry with a closed shell configuration (e^4 state). On the other hand, the Cr^{2-} center in 2*H*-SiC has a high-spin configuration. In this last case, our calculations showed that distortions were negligible.

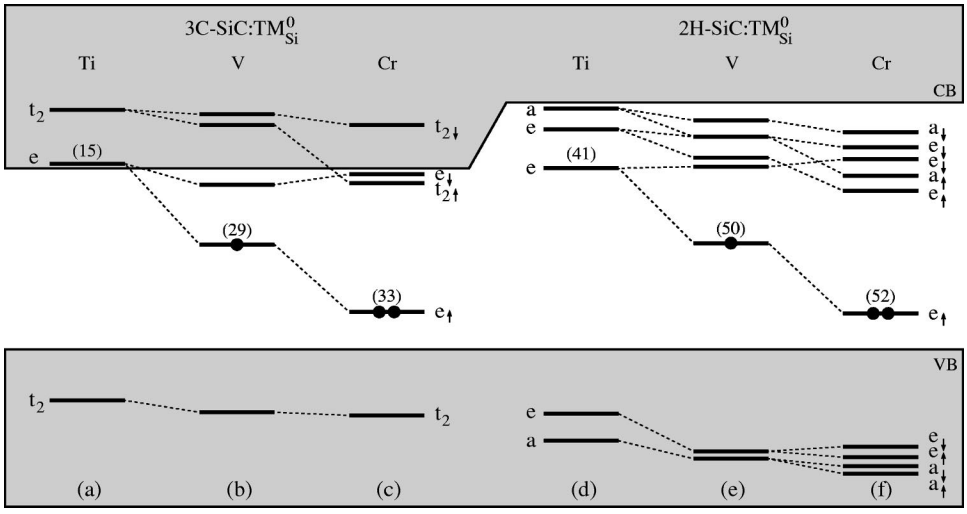

FIG. 4. Kohn-Sham energy eigenvalues representing the 3*d*-related impurity levels in the band gap region for the neutral substitutional Ti, V, and Cr, in the Si site, in 3*C*-SiC, (a)–(c), and 2*H*-SiC, (d)–(f). The valence-band top of 3*C* and 2*H* were aligned. Filled circles indicate the number of electrons in the highest occupied gap level, the ↑ and ↓ arrows represent the up and down spins, and the numbers in parenthesis give the *d*-character percentage of charge (inside the TM spheres with atomic sphere radius of 0.79 Å) in the *e* energy level. VB and CB symbols represent the valence and conduction bands, respectively.

TABLE II. Results for TM_{Si} in $3C$-SiC and $2H$-SiC in different charge states. The table presents the symmetry, total spin S, formation energies (ΔE_f with relation to the Ti^0 center in each polytype), transition energies E_t, and isotropic contact hyperfine terms A in ^{49}Ti, ^{51}V, and ^{53}Cr nuclei. The reference formation energies of Ti^0 are 4.3 eV and 2.8 eV in $3C$-SiC and $2H$-SiC, respectively. ε_F is the Fermi energy and $0.2 \leqslant \gamma \leqslant 1$. Energies and hyperfine parameters are given in eV and MHz, respectively.

	$3C$-SiC					$2H$-SiC				
	Symmetry	S	ΔE_f	E_t	A	Symmetry	S	ΔE_f	E_t	A
Ti^0	T_d	0	0.0		0	C_3	0	0.0		0
Ti^-						C_3	1/2	$2.7-\varepsilon_F$	2.7(0/−)	−22
V^+	T_d	0	$2.2+\varepsilon_F$	1.4(0/+)	0	C_3	0	$-0.7+\varepsilon_F$	1.4(0/+)	0
V^0	T_d	1/2	3.6		163	C_3	1/2	0.7		119
V^-	T_d	1	$5.2-\varepsilon_F$	1.6(0/−)	140	C_3	1	$2.5-\varepsilon_F$	1.8(0/−)	111
Cr^+	T_d	1/2	$6.7-0.2\gamma+\varepsilon_F$	0.5(0/+)	−40	C_3	1/2	$0.2-0.2\gamma+\varepsilon_F$	0.5(0/+)	−27
Cr^0	T_d	1	$7.2-0.2\gamma$		−36	C_3	1	$0.7-0.2\gamma$		−25
Cr^-	C_{3v}	3/2	$9.3-0.2\gamma-\varepsilon_F$	2.1(0/−)	−28	C_3	3/2	$2.9-0.2\gamma-\varepsilon_F$	2.2(0/−)	−22
Cr^{2-}	T_d	0	$11.8-0.2\gamma-2\varepsilon_F$		0	C_3	2	$5.4-0.2\gamma-2\varepsilon_F$	2.5(−/−2)	−20

Electron paramagnetic resonance (EPR) measurements in $4H$ and $6H$ polytypes[20,21] for V^0 and V^- assign spins, respectively, $S=1/2$ and $S=1$, and for Cr^+, Cr^0, and Cr^- spins, respectively, $S=1/2$, $S=1$, and $S=3/2$. Our calculated spin values for TM in $3C$ and $2H$ polytypes are fully consistent with those experimental data. On the other hand, EPR measurements for the Cr^{2-} in $6H$ find a spin $S=2$.[21] While our result for this center in $2H$ is consistent with such data, our result in the $3C$ polytype gives a spin $S=0$.

Table II also presents the transition energies for the centers. While acceptor transition energy levels for Ti impurity in hexagonal polytypes, $\varepsilon_v+3.13$ eV in $4H$ (Ref. 3) and $\varepsilon_v+2.90$ eV in $6H$,[22] have been observed, no Ti transition level has been measured in the cubic polytype.[3] These results for the acceptor transition should be compared to our value of $\varepsilon_v+2.7$ eV in $2H$-SiC. However, we should compare those transition energies with caution due to the different lattice structures of cubic and hexagonal SiC. While there is only one nonequivalent Si sublattice in $2H$-SiC, there are two and three nonequivalent Si sublattices in $4H$-SiC and $6H$-SiC, respectively. As a result, experimentalists find multiple TM-related transition energies.[23]

We find that the vanadium center (V_{Si}) is amphoteric in both $3C$ and $2H$ polytypes, which is consistent with experimental data in several polytypes.[20,24,25] For the donor transition, our value of $\varepsilon_v+1.4$ eV in both $3C$- and $2H$-SiC should be compared to the experimental values of $\varepsilon_v+1.7$ eV in $3C$-SiC and $\varepsilon_v+1.6$ eV in $6H$-SiC (Ref. 20). For the acceptor transition, our values (Table II) should be compared to experimental data values of $\varepsilon_v+(2.1–2.3)$ eV in $4H$-SiC (Refs. 24,25) and $\varepsilon_v+2.4$ eV in $6H$-SiC.[25] For the chromium center (Cr_{Si}), we find three transitions in $2H$-SiC and two in $3C$-SiC. The donor transition is in $\varepsilon_v+0.5$ eV in both $3C$- and $2H$-SiC polytypes and should be compared to the donor transitions in $4H$-SiC (Ref. 26) in $\varepsilon_v+0.54$ eV. Here we stress that Grillenberger *et al.*[23] have interpreted $\varepsilon_v+0.54$ eV as coming from the double donor Cr transition. This interpretation was made in order to be consistent with previous theoretical predictions in $3C$-SiC.[27] However, we believe that $\varepsilon_v+0.54$ eV should be assigned to the single-donor Cr transition (Fig. 6). To corroborate such assertion, by inspection of Table II, the difference between the donor and the acceptor transition is 1.6 eV in $3C$-SiC and 1.7 eV in $2H$-SiC. The experimental difference between donor and acceptor transitions in $4H$-SiC is 2.0 eV.[23] The Cr acceptor and double acceptor transitions are, respectively, at $\varepsilon_v+2.2$ eV and at $\varepsilon_v+2.5$ eV, which are consistent with experimental findings in $4H$-SiC.[23,28]

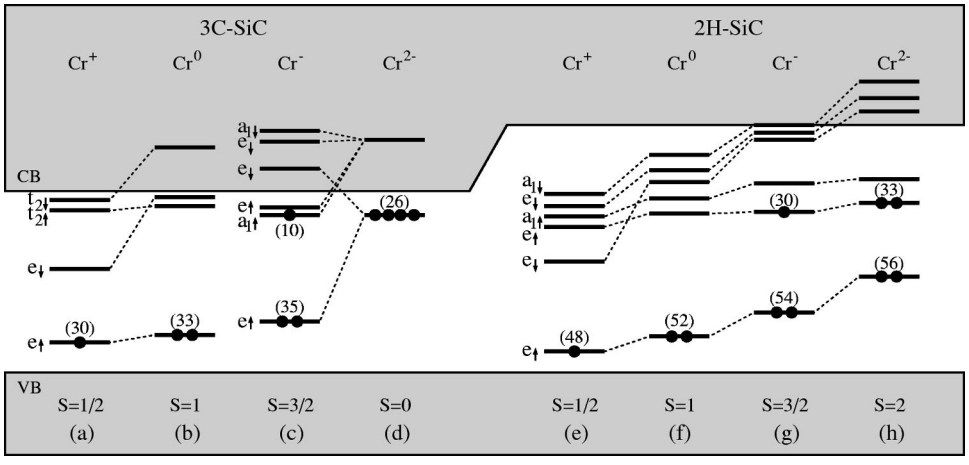

FIG. 5. Kohn-Sham eigenvalues representing the substitutional Cr in the Si site in $3C$-SiC, (a)–(d), and $2H$-SiC, (e)–(h). Filled circles indicate the electronic occupation in the gap levels, the ↑ and ↓ arrows represent the up and down spins, and the numbers in parenthesis give the *d*-character percentage of charge (inside the TM spheres with atomic sphere radius of 0.79 Å) in the occupied gap levels.

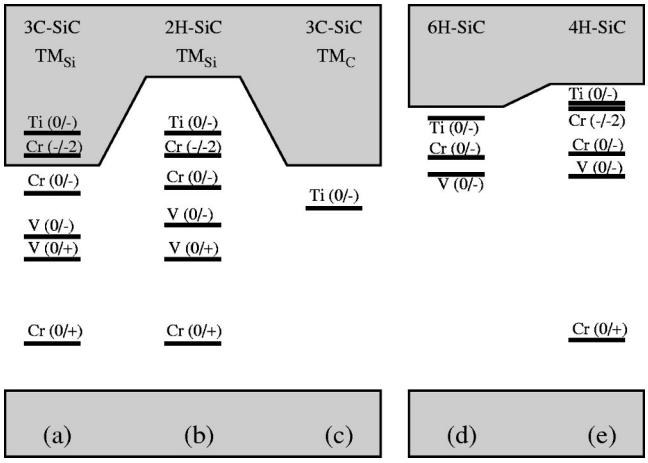

FIG. 6. Calculated acceptor and donor transition energies of Ti, V, and Cr in 3*C*-SiC (a), (c) and 2*H*-SiC (b). The figure also presents the available experimental transition energies (Ref. 23) in 6*H*- (d) and 4*H*-SiC (e). The valence-band offsets among all SiC polytypes are not considered, as described in the text.

Table II also presents the calculated contact hyperfine parameters for the TM_{Si} in 3*C*-SiC and 2*H*-SiC in several charge states. These results on the contact hyperfine parameters could be compared to experimental data,[20] presented in Table III, of transition metals in 4*H*- and 6*H*-SiC. Our results are in good agreement with the experimental values.

IV. SUMMARY

In summary, we performed a theoretical investigation of isolated Ti, V, and Cr impurities in hexagonal and cubic silicon carbide. We find that substitutional impurities (in the Si sublattice) are energetically more favorable than the interstitial ones. Our results for spin in several charge states and transition energies for substitutional TM are fully consistent with available experimental data. The chemical trends of neutral 3*d*-transition metals in SiC follow the typical trends of TM-related centers in semiconductors.[29,30] As the 3*d* level is filled, there is a deepening of the nonbonding *e* state with increasing of the impurity atomic number *Z*. The exchange splitting of this *e* level goes from 0.0 eV in Ti to 1.9 eV in Cr. The t_2 bonding level, which lies in the valence band, is only slightly influenced by variations of *Z*. On the other hand, the t_2 antibonding level is more strongly affected by *Z* changes. On going from V to Cr, the exchange splitting is such that it drives the TM center from a low- to a high-spin configuration, if distortions can be neglected.

TABLE III. Experimental hyperfine terms (Ref. 20) in the ^{49}Ti, ^{51}V, and ^{53}Cr nuclei in 4*H*- and 6*H*-SiC. The table presents the values for the impurity sitting in quasicubic (k_i) and hexagonal (h) sites. Terms are presented in MHz.

	4*H*-SiC		6*H*-SiC		
	k	h	k_1	k_2	h
$^{49}Ti^-$		42			
$^{51}V^-$	176	184	180	176	180
$^{51}V^0$		236	236, 188	236, 199	232, 267
$^{53}Cr^-$			26.5, 27	27.3, 28	

ACKNOWLEDGMENTS

The authors acknowledge financial support from Brazilian agencies FAPESP and CNPq. The calculations were partially performed at the LCCA-CCE of the Universidade de São Paulo.

APPENDIX IMPURITY FORMATION AND TRANSITION ENERGIES AND CHEMICAL POTENTIALS

The equilibrium concentration $[X]$ of an *X* impurity in a crystal depends upon its free energy

$$[X]=N_s\exp\{-\Delta_f G/k_B T\}, \tag{A1}$$

where N_s is the number of available sites, per unit volume, in the crystal where the impurity can occur, k_B is the Boltzmann constant, and *T* is the temperature. The free energy of formation (ΔG_f) is given by

$$\Delta_f G=\Delta_f E-T\Delta_f S+p\Delta_f V. \tag{A2}$$

Here, $\Delta_f E$, $\Delta_f S$, and $\Delta_f V$ are, respectively, the formation energy, the entropy variation, and the volume variation when the impurity is introduced into the system at a pressure *p*. The pressure ($p\Delta_f V$) and entropic ($T\Delta_f S$) terms can generally be neglected for typical defects in solid state.[31,32]

The formation energy of an *X* impurity in the *q* charge state in silicon carbide, $\Delta_f E^q$, is computed as

$$\Delta_f E^q=E(n_{Si},n_C,n_X,q)-n_{Si}\mu_{Si}-n_C\mu_C - n_X\mu_X+q(\mu_e+\varepsilon_v'), \tag{A3}$$

where $E(n_{Si},n_C,n_X,q)$ is the total energy of a supercell calculation containing n_{Si} silicon, n_C carbon, and n_X impurity atoms, and *q* is the charge state of the defect. μ_{Si}, μ_C, and μ_X are the chemical potentials for Si, C, and *X*, respectively. The electron chemical potential μ_e gives the position of the Fermi level in the band gap with relation to the valence-band top ε_v', and $0\leqslant\mu_e\leqslant\varepsilon_g$. $\varepsilon_v'=\varepsilon_v+\delta_q$, where δ_q lines up the band structures of the bulk material with and without the impurity, for each *q* charge state. This correction δ_q in the valence-band top is necessary due to the charge-density inhomogeneity in the finite primitive cell, which causes a Coulomb multipole interaction with its images, as discussed in Ref. 33.

The silicon and carbon chemical potentials are not independent. Considering both species in thermal equilibrium with SiC, their potentials are constrained by

$$\mu_{Si}+\mu_C=\mu_{SiC}, \tag{A4}$$

where μ_{SiC} is the energy of a SiC pair in the crystal. The allowed range of μ_{Si} and μ_C is determined by the heat of formation ($\Delta_f H$) of SiC, which is defined as

$$\Delta_f H^{SiC}=\mu_{SiC}-\mu_{Si}^{Bulk}-\mu_C^{Bulk}, \tag{A5}$$

which should be negative for stable compounds. Here, μ_{Si}^{Bulk} and μ_{C}^{Bulk} are the total energies per atom for Si and C crystals in the diamond structure, respectively. The calculated heat of formation for both 3*C*-SiC and 2*H*-SiC polytypes is -0.6 eV/SiC. This value is in good agreement with the experimental enthalpy of formation value of -0.68 eV/SiC.[13]

Depending on the growth conditions of SiC, the Si and C chemical potentials can vary according to

$$\mu_{Si} = \mu_{Si}^{Bulk} + \gamma \Delta_f H^{SiC}, \tag{A6}$$

$$\mu_{C} = \mu_{C}^{Bulk} + (1-\gamma) \Delta_f H^{SiC}, \tag{A7}$$

where γ is a parameter ranging from 0 (Si-rich condition) to 1 (C-rich condition).

For the case of transition metal impurities in SiC, the atomic chemical potentials could be determined as a function of their maximum values in the metallic phase and those potentials in the TM carbides (TM_mC_n, with *m* and *n* defining the atomic composition of the TM carbide):

$$m\,\mu_{TM} + n\mu_{C} = \mu_{TM_mC_n}. \tag{A8}$$

Combining this equation, for the case $m=n=1$, with Eqs. (A4) and (A6), and treating μ_{Si} as an independent variable, μ_C can be removed from Eq. (A8). Therefore, the TM chemical potential in SiC is given by

$$\mu_{TM}^{SiC} = \mu_{TMC} - \mu_{SiC} + \mu_{Si} = \mu_{TMC} - \mu_{SiC} + \mu_{Si}^{Bulk} + \gamma \Delta_f H^{SiC}. \tag{A9}$$

However, Eq. (A9) is only valid in the case that $\Delta_f H^{TMC} < \Delta_f H^{SiC}$. The calculated heat of formation of the TM carbides in the rocksalt structure are $\Delta_f H^{TiC} = -1.8$ eV, $\Delta_f H^{VC} = -1.0$ eV, and $\Delta_f H^{CrC} = +0.2$ eV. These results should be compared to the experimental values of $\Delta_f H^{TiC} = -1.91$ eV, $\Delta_f H^{VC} = -0.98$ eV, and $\Delta_f H^{CrC} = +0.02$ eV.[34]

Considering those limiting conditions, in the case of a Cr impurity in SiC, the chemical potential should be determined by the equilibrium with the Cr_3C_2 crystal. For that material, we used the experimental heat of formation, $\Delta_f H^{Cr_3C_2} = -0.855$ eV,[34] together with the energy of the calculated elemental phase. In this case, the variation of Cr chemical potential is

$$\mu_{Cr} - \mu_{Cr}^{Bulk} = \tfrac{1}{3}\Delta_f H^{Cr_3C_2} - \tfrac{2}{3}(1-\gamma)\Delta_f H^{SiC}. \tag{A10}$$

Since the $\mu_{Cr} - \mu_{Cr}^{Bulk} \leqslant 0$ condition must be satisfied, γ can only vary in the range $0.2 \leqslant \gamma \leqslant 1$.

The transition energy E_t of a center can be obtained from the formation energy of the center at different charge states. For example, for the transition energy $(q+1/q)$ we should have $\Delta_f E^{q+1} = \Delta_f E^q$, and E_t is given by

$$E_t(q+1/q) \equiv \varepsilon_F = E(n_{Si}, n_C, n_X, q+1) - E(n_{Si}, n_C, n_X, q) - q\,\delta_q + (q+1)\,\delta_{q+1}. \tag{A11}$$

[1] M.A. Capano and R.J. Trew, MRS Bull. **22**, 19 (1997).
[2] N.W. Jepps and T.F. Page, Prog. Cryst. Growth Charact. **7**, 259 (1983).
[3] A.A. Lebedev, Semiconductors **33**, 107 (1999).
[4] T. Dalibor, G. Pensl, H. Matsunami, T. Kimoto, W.J. Choyke, A. Schoner, and N. Nordell, Phys. Status Solidi A **162**, 199 (1997).
[5] J.M. Langer and H. Heinrich, Phys. Rev. Lett. **55**, 1414 (1985).
[6] D.J. Singh, *Planewaves, Pseudopotentials and the LAPW Method* (Kluwer Academic, Norwell, 1994).
[7] P. Blaha, K. Schwarz, and J. Luitz, computer code WIEN97 (Karlheinz Schwarz, Techn. Universität Wien, Wein, Austria, 1999).
[8] R. Larico, L.V.C. Assali, W.V.M. Machado, and J.F. Justo, Appl. Phys. Lett. **84**, 720 (2004).
[9] P. Hohenberg and W. Kohn, Phys. Rev. **136**, B864 (1964).
[10] W. Kohn and L.J. Sham, Phys. Rev. **140**, A1133 (1965).
[11] J.P. Perdew, S. Burke, and M. Ernzerhof, Phys. Rev. Lett. **77**, 3865 (1996).
[12] H.J. Monkhorst and J.D. Pack, Phys. Rev. B **13**, 5188 (1976).
[13] *Numerical Data and Functional Relationships in Science and Technology*, edited by O. Madelung, M. Schulz, and H. Weiss, Landolt-Börnstein, New Series, Group III, Vol. 17, pt. A (Springer-Verlag, New York, 1982).
[14] M.S. Miao and W.R.L. Lambrecht, Phys. Rev. B **68**, 125204 (2003).
[15] K.O. Barbosa, W.V.M. Machado, and L.V.C. Assali, Physica B **308-310**, 726 (2001).
[16] L.V.C. Assali, W.V.M. Machado, and J.F. Justo, Physica B **340-342**, 116 (2003).
[17] L. Patrick and W.J. Choyke, Phys. Rev. B **10**, 5091 (1974).
[18] A. Qteish, V. Heine, and R.J. Needs, Phys. Rev. B **45**, 6534 (1992).
[19] A.O. Evwaraye, S.R. Smith, and W.C. Mitchel, Appl. Phys. Lett. **67**, 3319 (1995).
[20] J. Baur, M. Kunzer, and J. Schneider, Phys. Status Solidi A **162**, 153 (1997), and references therein.
[21] P.G. Baranov, I.V. Il'in, E.N. Mokhov, and V.A. Kramtsov, Phys. Solid State **41**, 783 (1999).
[22] Yu.M. Suleimanov, I. Zaharchenko, and S. Ostapenko, Physica B **308-310**, 714 (2001).
[23] J. Grillenberger, N. Achtziger, G. Pasold, and W. Witthuhn, Mater. Sci. Forum **389-393**, 573 (2002), and references therein.
[24] W.C. Mitchel, R. Perrin, J. Goldstein, A. Saxler, M. Roth, S.R. Smith, J.S. Solomon, and A.O. Evwaraye, J. Appl. Phys. **86**, 5040 (1999).
[25] S.A. Reshanov and V.P. Rastegaev, Diamond Relat. Mater. **10**, 2035 (2001).
[26] G. Pasold, N. Achtziger, J. Grillenberger, and W. Witthuhn, Mater. Sci. Forum **353**, 471 (2000).
[27] H. Overhof, Mater. Sci. Forum **258-263**, 677 (1997).

[28] N. Achtziger and W. Witthuhn, Phys. Rev. B **57**, 12 181 (1998).
[29] L.V.C. Assali and J.F. Justo, Phys. Rev. B **58**, 3870 (1998).
[30] J.F. Justo and L.V.C. Assali, Int. J. Mod. Phys. B **13**, 2387 (1999).
[31] C.G. Van de Walle, D.B. Laks, G.F. Neumark, and S.T. Pantelides, Phys. Rev. B **47**, 9425 (1993).
[32] A. Zywietz, J. Futhmüller, and F. Bechstedt, Phys. Rev. B **59**, 15 166 (1999).
[33] T. Matilla and A. Zunger, Phys. Rev. B **58**, 1367 (1998).
[34] A.F. Guillermet and G. Grimvall, J. Phys. Chem. Solids **53**, 105 (1992).